Heliyon 9 (2023) e13920

Contents lists available at ScienceDirect

Heliyon

journal homepage: www.cell.com/heliyon

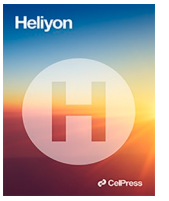

Research article

A numerical study of COVID-19-laden droplets dispersion in aircraft cabin ventilation system

Zhuxun Liu [a], Jingyi Wu [a,*], Guang Yang [a], Xintai Zhang [b], Zheng Dai [b]

[a] School of Mechanical Engineering, Shanghai Jiao Tong University, Shanghai 200240, China
[b] COMAC Shanghai Aircraft Design & Research Institute, Shanghai 201203, China

ARTICLE INFO

Keywords:
Virus (COVID-19)-laden droplets
Computational fluid particle dynamics (CFPD)
Cough
Ventilation system
Infection probability

ABSTRACT

Ventilation systems for aircraft cabins are mainly used to maintain a comfortable environment in the cabin and ensure the health of passengers. This study evaluates the decontamination performance of two cabin ventilation systems, the displacement ventilation (DV) system and the mixing ventilation (MV) system, in preventing contamination by virus (COVID-19)-laden droplets. The Euler-Lagrange method was used to computationally model droplet dispersion of different diameters and their behavior in the two systems was contrastively analyzed. Statistics on droplet suspension ratios and duration as well as the infection probability of each passenger were also computed. It was found that11.07% fewer droplet remained suspended in the DV system were than those in the MV system 10s from droplet release. In addition, the number of droplets extracted from the exhausts in the DV system was 13.15% more than the MV system at the 400s mark. In the DV system, higher ambient wind velocities were also found to locally increase infection probability for passengers in certain locations.

1. Introduction

The large-scale and sustained outbreak of novel coronavirus COVID-19 in 2019–2022 has brought to the fore the need to prevent and control airborne virus transmission. Airborne disease transmission through droplets and aerosols contribute significantly to spread of infectious diseases [1], particularly in artificially ventilated enclosed spaces, such as aircraft, with numerous cases of the COVID-19 being communicated via airborne transmission in flights [2]. Available evidence suggests that persons infected with COVID-19 transmit it to others by discharging tiny droplets carrying the virus when they talk, sneeze, cough, and even breathe [3–6]. Hence, the behavior and spread of virus (COVID-19)-laden droplets in aircraft cabin ventilation systems needs to be studied further.

The characteristics of air and droplets emitted during human breathing have been much examined in the literature, with Mie interferometric graphs being used to measure the size and dispersion of droplets, and image velocimetry being used to measure air velocity in flow fields [7]. Droplets exhaled by the human body are multi-component, including evaporable liquid water and non-volatile substances, lipids, proteins, sugars, and sodium chloride [8]. Early evaporation tests suggest that droplets consist of 93.2% water and 6.8% aforementioned non-volatile substances [9]. Christian et al. (2021) [10] computed the relationship between initial and final droplet size after evaporation in an acoustic levitation and argued that equilibrium droplet size in general approximated 20% of initial diameter. Nonetheless, the literature [8] shows that the final size of droplets is related to the amount of saliva non-volatiles in the subject. Moreover, the evaporation process is affected by ambient temperature and humidity [11]. The evaporation process

* Corresponding author.
E-mail address: jywu@sjtu.edu.cn (J. Wu).

https://doi.org/10.1016/j.heliyon.2023.e13920
Received 10 July 2022; Received in revised form 14 February 2023; Accepted 15 February 2023
Available online 23 February 2023

changes the diameter of the droplets; it also affects the diffusion of the droplets.

The pattern of cough transmission from a single person has been considered in many literatures [7,10,12]. Yan et al. (2019) [13] found that small droplets of 3.5 μm–20 μm in diameter would be lifted by the heat plume flow from the human body in enclosed space; medium droplets (10–100 μm) and very small droplets (<5–10 μm) are more affected by ambient winds from the perspective of computational fluid particle dynamics (CFPD); and larger droplets (≥50 μm) follow a ballistic trajectory and are unable to be carried into the breathing zone. In addition, studies of the human respiratory tract [14] have found that particles smaller than 10 μm can enter the lower respiratory tract and lungs, while particles larger than 10 μm are more often trapped in the upper respiratory tract. Therefore, some scholars [15,16] have used 10 μm as the truncation diameter of the upper and lower respiratory tracts. Furthermore, research recently published by the U.S. Transportation Command (USTRANSCOM) and the Air Mobility Command (AMC) shows that droplet dispersion from a patient is localized in the cabin space, primarily affecting the patient's row and the individuals in the patient's front and rear rows [17].

Due to its structure and dense population [18], aircraft cabin space is prone to airborne transmission; therefore, the selection and optimization of suitable ventilation systems must be studied. The ventilation system currently widely used in commercial aircraft is the mixing ventilation (MV) system, where the regulated airflow enters the cabin at a certain velocity from the ceiling or top of the sidewall, and the airflow leaves the cabin through an outlet near the floor [19]. However, previous studies have found that the MV system has poor control over pollutants [20–22], so more and more research is starting to focus on the development of displacement

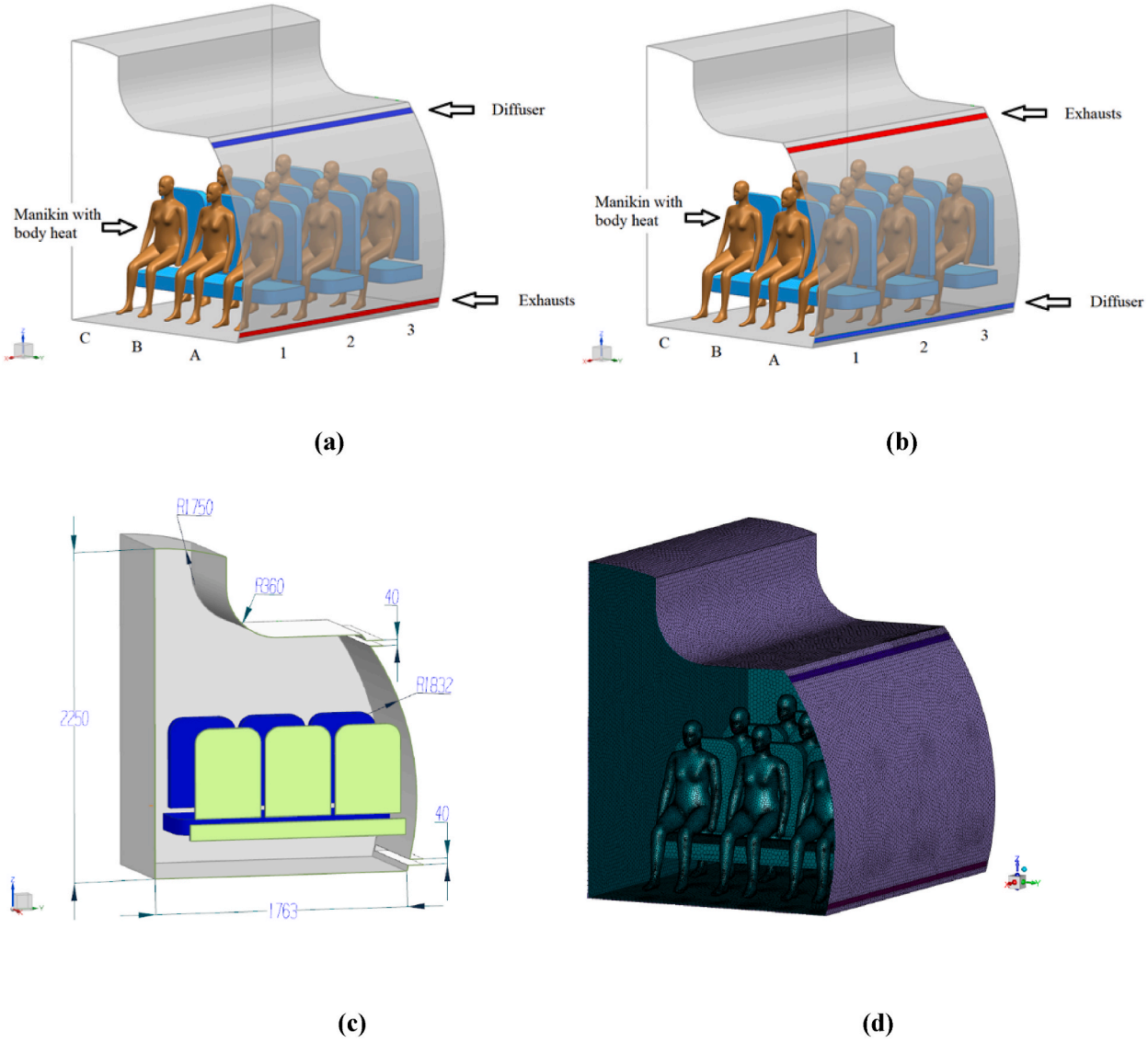

Fig. 1. Dimensions of the Aircraft Cabin. (a)Aircraft cabin with DV system, (b) Aircraft cabin with MV system, (c) The size of computational domain, (d)Mesh of computational domain.

ventilation (DV) systems [23]. DV systems employ lower airflow velocity dispersion, with inlets generally arranged at the lower sidewalls of the nacelle, while outlets are arranged near the *trans*-ceiling [24].

Current research on ventilation systems generally suggests that the DV system is superior to the MV system in terms of preventing pollution discharge. However, at present, there is little high-precision experimental data on the dispersion of droplets in DV and MV ventilated cabins. Most existing physical studies involve very few measurement points [25,26], as they are based on Mie scattering theory as the principle of measurement risk destruction of the native flow field by introducing too many measurement points.

Numerical study was conducted to investigate the transport of jet droplets in a seven-row extended cabin by Gupta et al. (2011) [27]. Conclusions in detail was reached by investigating the transport of droplets from respiration and coughing. The risk of influenza transmission was further explored with one indicator patient in seven rows of passenger cabins [28]. They choose two different methods, deterministic and probabilistic, to measure influenza risk. Those studies provide an important theoretical basis for subsequent CFD (computational fluid dynamics) research. Due to the limited computational resource, the passenger model is oversimplified to a combination of blocks in the simulated cabin for pollutant transport.

Yan et al. (2017) [29] gave a detailed description of the distribution of pollutants in the cabin and studied the differences in the distribution of pollutants among infected people in different positions. However, in their study, the initial diameter distribution of particles was oversimplified and the evaporation of particles was ignored, and the ventilation system's influence had not been discussed.

In the past, the research indexes of ventilation system mainly focused on pollutant removal and human thermal comfort [30–32]. However, in the current epidemic situation, it is urgent to take infection probability as the main index of the ventilation system. While previous infection probability studies [29,33] focused on the change of passenger position, but ignored the influence of ventilation system itself on the transmission of pollutants.

Based on the Euler-Lagrangian method, this study simulated the trajectory of droplet pollutants, and the fate of pollutant droplets at different times was analyzed under different ventilation systems. The Lagrangian-based Wells-Riley approach as a risk assessment indicator to re-examine the two ventilation systems in the cabin. By comparing the advantages and disadvantages of different ventilation systems, we found the DV system was not superior to the MV system locally. The influence of the ventilation system and wind velocity on infection probability was studied. The results of this study will provide inspiration for the improvement of ventilation system optimization in the future.

2. Method

2.1. Geometry and meshing

Using 3D CFD modeling, a model of the cabin segment of the aircraft is built, with a maximum spatial size of 2.90 m × 2.08 m × 2.25 m. The specific geometries are shown in Fig. 1. Fig. 1 (a) shows the aircraft cabin with DV system, and Fig. 1 (b) shows the aircraft cabin with MV system. Talaat et al. (2021) [52] found particulate pollutants released by human beings were mainly distributed in three rows, therefore, only three seat rows were modelled to reduce computational load. Each seat is decorated with a manikin, which was obtained from an open database (https://www.cfd-benchmarks.com/). Again, due to limited computing power, appropriate simplifications are made to the models [34], Specifically, reasonable conditional assumptions are made to achieve a certain degree of simplification of the calculation process while maintaining reasonable precision. A mouth opening is also created for each manikin with hydraulic diameters equivalent to 19.5 mm. Due to the symmetrical dispersion of the airflow field, only one half of the chamber is simulated. The cabin walls, ceiling and trunk are simplified as curved surfaces, while the seat handles, seat legs and windows are ignored. Fig. 1 (c) illustrates the main geometric dimensions of the aircraft.

2.2. Governing equations

A well-validated CFPD model [13,35,36] is used to model the continuous air and the evaporation process of liquid droplets. The continuous phase is described by Euler equations, and the internal air flow field is modelled using numerical methods to create a Navier-Stokes equation system containing mixed terms, with the following control Eqs. (1)–(4):

$$\frac{\partial}{\partial t}\left(\rho_{mix}\alpha_{air}\right)+\nabla\cdot\left(\rho_{mix}\alpha_{air}\vec{U}_{mix}\right)=0 \tag{1}$$

$$\frac{\partial}{\partial t}\left(\rho_{mix}\alpha_{vap}\right)+\nabla\cdot\left[\rho_{mix}\alpha_{vap}\vec{U}_{mix}-\rho_{mix}D_k\left(\nabla\alpha_{vap}\right)\right]=S_{vap} \tag{2}$$

where ρ_{mix} is the density of the moist air; α_{air} is the mass fraction of the dry air; α_{vap} is the mass fraction of the water vapor; $\vec{U}_{mix}$ is the velocity of the moist air; D_k is the dispersion rate of the water vapor in the moist air; S_{vap} is the water vapor source generated by the evaporation of droplets.

$$\frac{\partial}{\partial t}\left(\rho_{mix}\vec{U}_{mix}\right)+\nabla\left\{\rho_{mix}\vec{U}_{mix}\vec{U}_{mix}-\mu\left[\nabla\vec{U}_{mix}+\left(\vec{U}_{mix}\right)^{T}\right]\right\}=\vec{F}_{md}-\nabla P+S_{buoy} \tag{3}$$

$$\frac{\partial}{\partial t}(\rho_{min}H_{mix}) + \nabla \cdot \left[\rho_{mix}\overrightarrow{U}_{mix}H_{mix} - \nabla(\lambda_{mix}T_{mix})\right] = Q_{md} \tag{4}$$

The Lagrange method is used to track the transport and trajectories of discrete phase droplets, as shown in the following formula (5):

$$m_d\frac{d\overrightarrow{U}_d}{dt} = \overrightarrow{F}_D + \overrightarrow{F}_{Bouy} + \overrightarrow{F}_{BM} \tag{5}$$

where $\overrightarrow{F}_D$ is drag force, and $\overrightarrow{F}_{Bouy}$ is buoyancy, and $\overrightarrow{F}_{BM}$ is the Brownian motion force.

The drag force $\overrightarrow{F}_D$ is defined as formula (6):

$$\overrightarrow{F}_D = \frac{C_D}{2}\frac{\pi d_d^2}{4}\rho_{mix}\left|\overrightarrow{U}_d - \overrightarrow{U}_{mix}\right|\left(\overrightarrow{U}_d - \overrightarrow{U}_{mix}\right) \Big/ C_c \tag{6}$$

where d_d is the diameter of the droplet, and C_c is the Cunningham correction coefficient, which is used to correct the slip condition which can be caused by the scale of droplets.

The drag coefficient C_D is defined as formula (7):

$$C_D = a_1 + \frac{a_2}{Re_d} + \frac{a_3}{Re_d^2} \tag{7}$$

where a_1, a_2 and a_3 are determined by the Reynolds number of droplets.

The buoyancy force $\overrightarrow{F}_{Bouy}$ is defined as formula (8):

$$\overrightarrow{F}_{Bouy} = \frac{\pi d_d^3}{6}(\rho_d - \rho_{mix})g \tag{8}$$

And $\overrightarrow{F}_{BM}$ is considered negligible at the current size.

Based on the available literature [13], it was directly assumed that the initial composition ratio of saliva is 1.8% non-volatile solid mixture and 98.2% vaporizable water. Evaporation is controlled by judging the relationship between the partial pressure of water vapor and the saturated vapor pressure on the surface of the droplet. Mathematically, evaporation is mainly determined by the diffusion mechanism and mass transfer rate, as shown in the following formula (9):

$$\frac{dm_d}{dt} = -\frac{dS_{vap}}{dt} = -\pi d_d D_{dyn} Sh \frac{M_v}{M_m} ln\frac{P - P_{v,s}}{P - P_{v,m}} \tag{9}$$

where D_{dyn} is the dynamic diffusion rate of water vapor in the continuum; Sh is the Sherwood number; the molecular weights of the vapor and the mixed air are expressed as M_v, M_m respectively; P is the pressure of local environment; $P_{v,s}$ is the partial pressure of the water vapor on the droplet surface; and $P_{v,m}$ is the partial pressure of the droplet and the air mixture.

The Phase change latent heat transfer is modelled as formula (10):

$$m_d C_{p,d}\frac{dT_d}{dt} = q_{md} - h_{lv}\frac{dm_d}{dt} \tag{10}$$

where q_{md} is the heat exchange rate at interface; h_{lv} is the particulate matter latent heat; Supposing the temperature gradient inside the droplet is ignored.

2.3. Model verification

As shown in Table .1 that most of the previous research to simulate the flow field in the aircraft cabin used the RNG k-ε model, which results have been made comparison and demonstration with the PIV experimental data.

Table 1
Summary of CFD validation experiments for aircraft cabins.

Authors	Platform	Instruments	Validated numerical methods
Zhang et al., 2009 [20]	B767 mock-up (occupied)	One UA	RNG k-ε
Zítek et al., 2010 [53]	B767 mock-up (occupied)	PIV (helium bubbles)	Standard k-ε
Liu et al., 2013 [54]	First class of MD-82 (occupied)	–	RNG k-ε
Yan et al., 2017 [29]	Boeing 737-200	Exp. data with similar conditions	RNG k-ε
Zhao et al., 2019 [35]	Rectangular space	–	SST k-w
Haghnegahdar et al., 2010 [45]	Respiratory tract model	Exp. data with similar conditions	SST k-w
Yu et al., 2020 [36]	Rectangular space	–	SST k-w

The SST k-ω model was used in the research for calculating droplet propagation in the respiratory flow field and hypothetical scenario. Laminar-to-turbulence airflow field predictions using the SST k-ω transition model [37]. Specifically, comparisons of airflow velocity magnitude and iso-surfaces show good matches between the employed SST k-ω transition model and the experimental measurements [38] have been done in the same subject-specific human airway model.

In order to compare the differences between the two turbulence models in the cabin, we use the experimental data [39] as the comparison. The supply air volume was controlled to be 9.4 L/(s· person), as recommended by ASHRAE (2007) [40]. Since passengers are the main heat source in the cabin, a convective heat load of 22.83 W/m^2 was applied at each manikin.

From Fig. 2 (a)&(b)&(c) we found that the RNG k-ε model is better fit the experimental results in our calculation model. Fig. 2 (d) shows the position of each line.

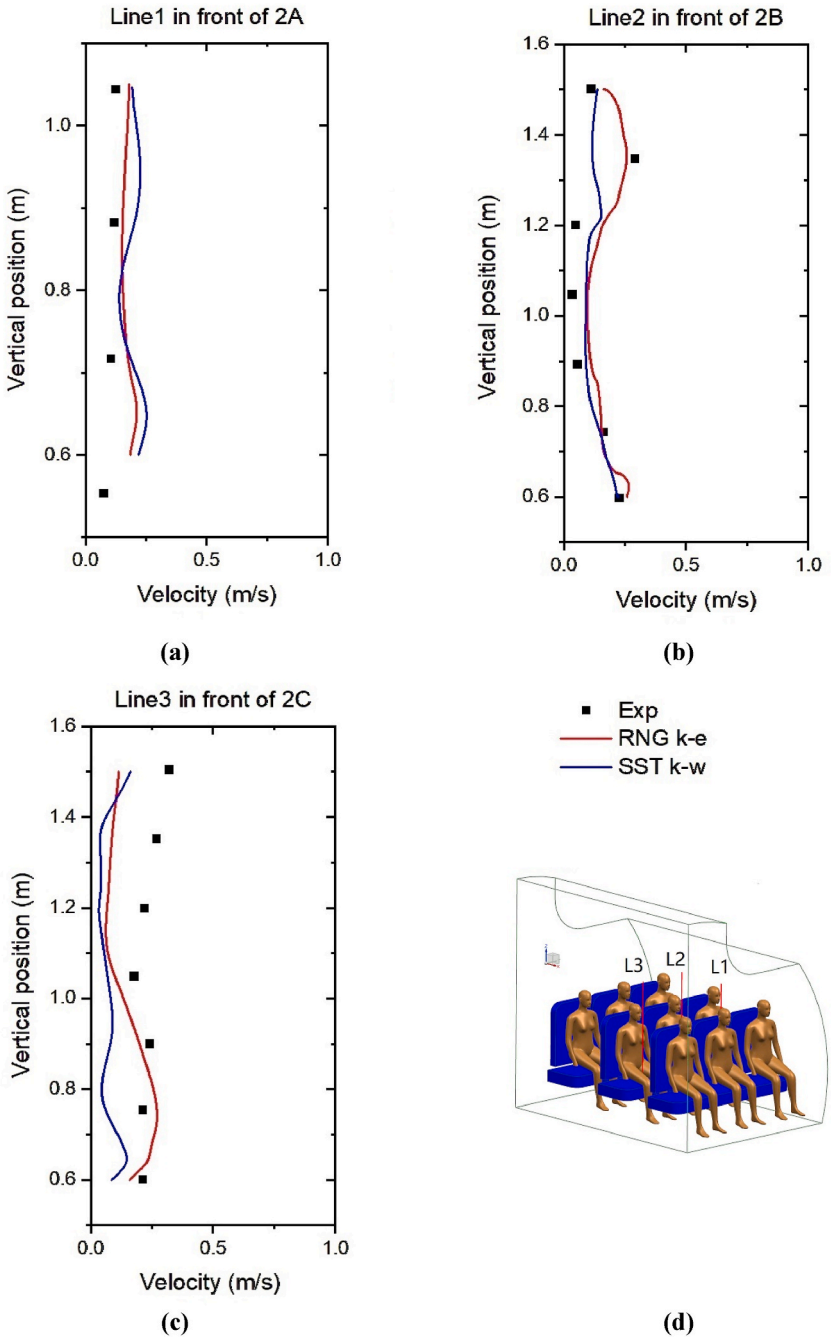

Fig. 2. Comparison of velocity profiles between numerical predictions and experimental measurements (a) L1, (b) L2, (c)L3, (d)Diagrammatize.

(1) Considering the main particle size used in this study is 10 μm of the discrete term, which have a high flow field following, the accuracy flow field velocity would determine the accuracy of the calculation result.
(2) The relative humidity in the cabin is controlled below 20% [41], the particle evaporation rate is fast, and the particles can reach the equilibrium state in a very short time.

Therefore, in order to predict the particle trajectory more accurately in susceptible's breath zone, we chose RNG k-ε model for calculation.

The domains were discretized with a Polly-Hexcore mesh (Fig. 1 (d)), which was projected on the surface of the manikins and nearby walls to ensure $y^+ < 1$. In order to verify the independence of the results from the mesh, coarse, medium, and fine meshes were chosen for comparison. The detailed mesh statistics and information are shown in Table 2.

The velocity comparison was set for a straight segment L0 of 1.1 m length and parallel to the board. It can be seen from Fig. 3 that changing the mesh density did not cause a significant difference in the air velocity dispersion in L0. Considering fluctuations in velocity, the maximum velocity error between the medium and fine mesh is only 0.03 m/s. Given the acceptable range, the medium size was chosen to balance accuracy and computational efficiency.

2.4. CFPD validation model

The evaporation process of the continuous and discrete phase models was verified separately to ensure the accuracy and reliability of the entire model. When validating the evaporation process of the discrete term, a simple calculation model was separately set up to verify the evaporation rate.

The evaporation model used in this case relied on the relative humidity and temperature in the environment. It was assumed that the volatile substance content of the multi-component droplet solution is 98.2%, while the non-volatile substance content is 1.8% [13]. The boundary conditions are listed in Table 3.

As shown in Fig. 4, the error of the simulated model compared to a reference experiment [42] was within a controllable range. The error in the time consumed for evaporation from the initial droplet size to a certain diameter is also acceptable. It can also be seen from the figure that the ratio of the final droplet diameter to the initial diameter is 1:4. In the simulation, the time it took for the 100 μm droplet to evaporate to non-volatile substance is about 6.4s, while a 10 μm droplet took only 0.065s for its volatile parts to evaporate completely.

2.5. Boundary conditions

The outlet of the ventilation unit is set as the pressure outlet and the inlet of the ventilation is set as the velocity inlet. The center plane (Y = 0 m) is set as a symmetric plane, and symmetric boundary conditions are applied on the axial section of the aircraft cabin. The mouths of the nine manikins are set as velocity inlets. The visible wall surface is set to trap mode, with deposits occurring as soon as droplets touch the seat, bulkhead, floor, luggage compartment, or the human body; exhausts and air inlets were set to escape mode, with droplets recorded as they leave the outlet. The trap or escape boundary condition means that the boundary acts as a sink for the droplet mass when it hits the wall [43]. To generate thermal buoyancy flow, the surface temperature of the human body is set to 327 K and the equivalent heat flux [44] set to 22.83 W/m^2. The initial temperature of the cabin is 298 K, radiative heat transfer in the cabin is ignored, and the other walls' temperatures are assumed consistent with the ambient temperature.

Since the discrete phase in the flow field does not have periodic characteristics, the sliding wall boundaries in the front and rear spaces were used to make the continuous flow field retain periodic characteristics, while the left side of the model uses symmetrical surfaces. The sliding wall boundary means the wall has no shear force with the fluid. For several reasons, periodic boundary conditions are not used on the front and back boundaries, some of which are: (1) Discrete phase do not have periodicity on the front and back boundaries; (2) Periodic conditions cannot be used simultaneously with the DPM model; (3) periodic boundary conditions bring about non-physical sedimentation of droplets. Setting the front and rear walls as a sliding wall surface, adopting an escape mode for the action of discrete phase, and increasing the number of seat rows to three rows improved the simulation accuracy of droplet dispersion in the cabin.

In order to accurately simulate the airflow field and discrete term dispersion generated by passenger's coughing and breathing, the experimental data [29,45] is selected and fitted (Fig. 5 (a)&(b)), and then the fitted equations used as boundary conditions. At the beginning of the calculation, the flow field of the ventilation system is first calculated. After the flow field stabilized, droplets are emitted from the mouth of the manikin in 2B (Fig. 1). The other uninfected passengers maintain a normal breathing pattern, and the breathing phase differences in the patterns are random. Coughing behavior is accompanied by the release of droplets. For different research contents, two boundary conditions are used:

Table 2
Mesh independence verification generates information.

Mesh type	Minimum mesh size (mm)	The number of nodes
Coarse	8	5, 808, 072
Medium	4	9, 736, 293
Fine	2	12, 345, 632

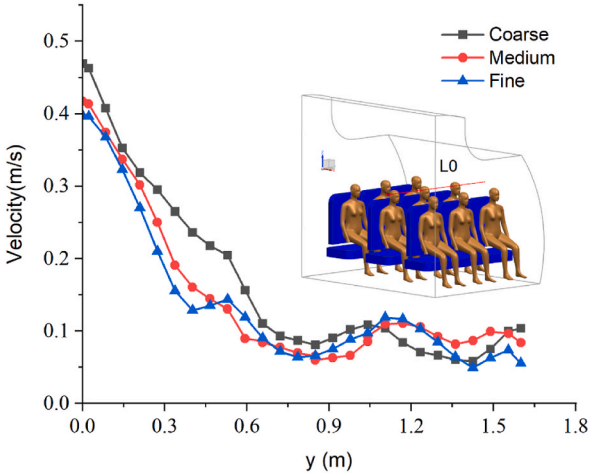

Fig. 3. Mesh Independence Verification results.

Table 3
Validation model boundary conditions.

Boundary conditions	The parameter value
Inlet velocity	0.1 m/s
Droplet size	10 μm, 100 μm
Temperature	25 °C
Type of injection	Single
Relative humidity	0%

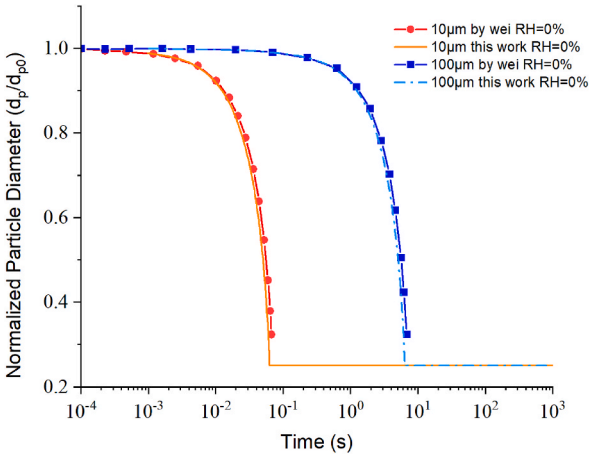

Fig. 4. Validation of evaporation modeling.

(1) Seven droplet sizes (1 μm, 2.5 μm, 5 μm, 10 μm, 30 μm, 50 μm, 100 μm) are tested. To pass the dimensionless sensitivity test [29] for particles number, the number of droplets released is 10000 of each droplets size.
(2) In the calculation of infection probability, we use the monodisperse distribution defined by Weibul's probability density function (shown in Fig. 5(c)) for the calculation of the passenger infection probability [46].

2.6. *Probability of infection assessment method*

It is considered in the literature that the degree of COVID-19 infection is positively correlated with the amount of infectious agents that susceptible are exposed to Ref. [36]. In order to evaluate the risk of local infection in the DV and MV systems, a previous calculation method for inhalation area [47] was improved. The trajectory of droplets was counted in the hemispherical area (Fig. 5(d)) with a radius of R in front of each passenger's mouth. This value represents the infection probability of the passenger.

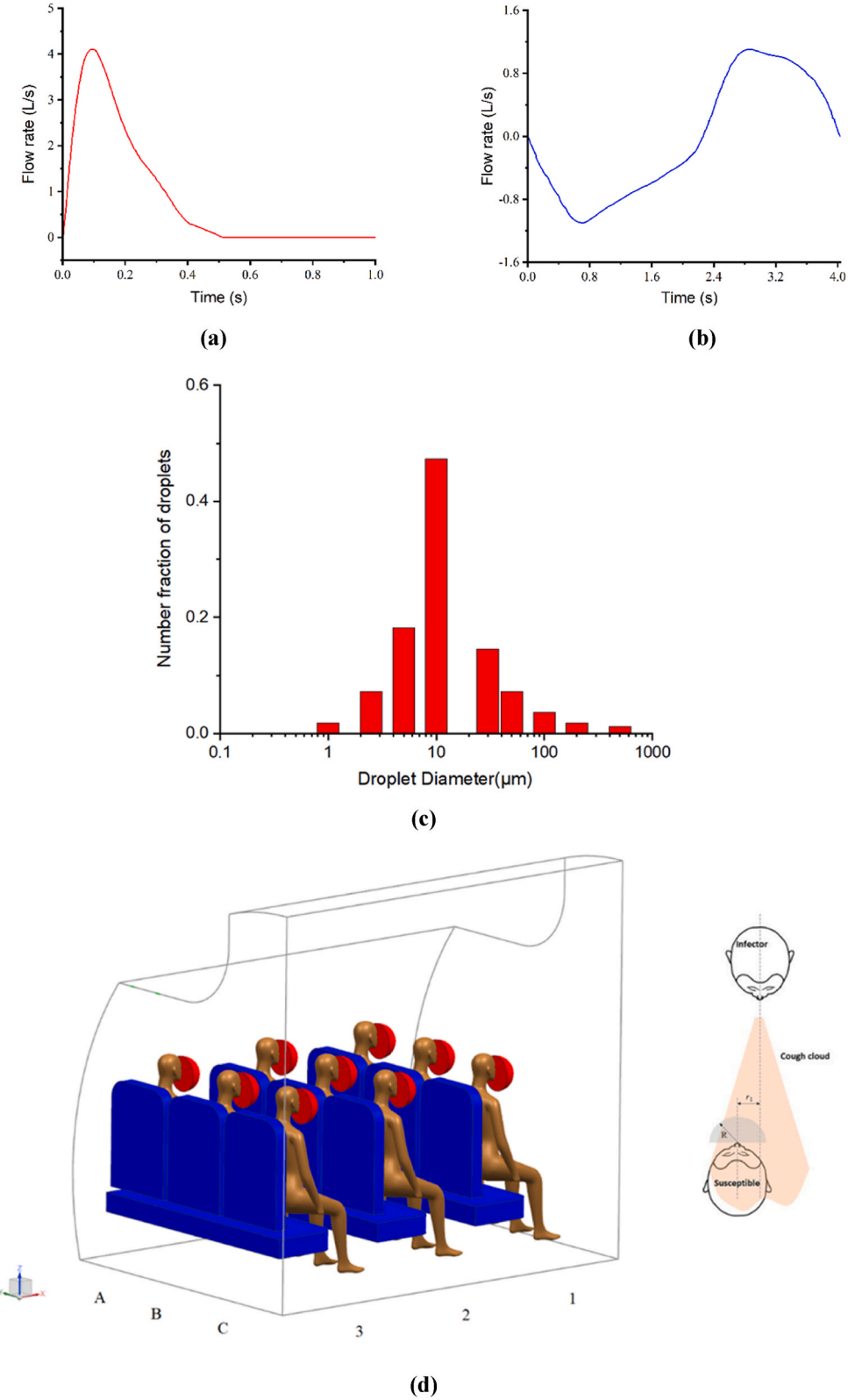

Fig. 5. Boundary conditions at the outlet of the human mouth. (a) Cough, (b) Breathing, (c) Initial droplet diameter distribution, (d)Diagrammatize of the inhalation area.

The Wells-Riley model has been widely used to assess the risk of respiratory disease transmission, as shown in Eq. (11). A quantum refers to the quantity of discrete term matter needed to infect a normal person. It can consist of numbers of particles that are thought to be randomly distributed in the air of a closed space [48].

$$P = \frac{C}{S} = 1 - exp\left(-\frac{Iqpt}{Q}\right) \tag{11}$$

Where P is the infection probability for the susceptible, C is the quantity of infection cases, S is the quantity of susceptibles, I is the quantity of infectors, q is the generation rate of quanta ($quanta/h$), p is the individual lung ventilation rate (m^3/h), t is the time interval of exposure (h), and Q is the ventilation rate (m^3/h).

The CFD-integrated Wells-Riley model was applied by many researchers [28,29,49]. particle source in-cell (PSI–C) scheme based on Lagrange method can integrate the mass of fine particle over time to obtain the concentration of the discrete phase in cell [29], as shown in Eq. (12):

$$\overline{C}_j = \left(\frac{M\sum_{i=1}^{n} dt_{ij}}{V_j}\right) \tag{12}$$

where M is the mass flow rate in each particle trajectory, V_j is the volume of the calculated volume cell, dt_{ij} is the time that particle i spends in trajectory in cell j.

The calculated concentrations of pollutants inhaled by susceptible populations can be used to determine the risk of infection for each susceptible population as Eq. (13) [49,50]:

$$P_i = 1 - exp\left(-C_{q,i}\, pt\right) \tag{13}$$

where P_i is the infection probability for the susceptible i, $C_{q,i}$ is the concentration of pollutants inhaled by susceptible i, p is the respiratory flow rate of susceptible, and t is the individual exposure time.

3. Results and discussion

3.1. Analysis of flow fields in different ventilation systems

From the velocity contours of the air flow field in Fig. 6, it was found that in the DV system (Fig. 6 (a)), the flow field is mainly vertical upward near the passenger's body in the 2A position (Fig. 1), which is consistent with the direction of the heat plume of human body. Moreover, the forced convection caused by the ambient wind enhances the convection on the human body, while the flow between the passenger's body in the 2B and 2C positions (Fig. 1) was vertically downward. The contours also indicated that the forced convection caused by the ambient wind suppresses the heat plume near the human body. When the simulated flow field was compared with the PIV experiment results in the literature [51], the errors (shown in Fig. 7) were within an acceptable range. Their model and

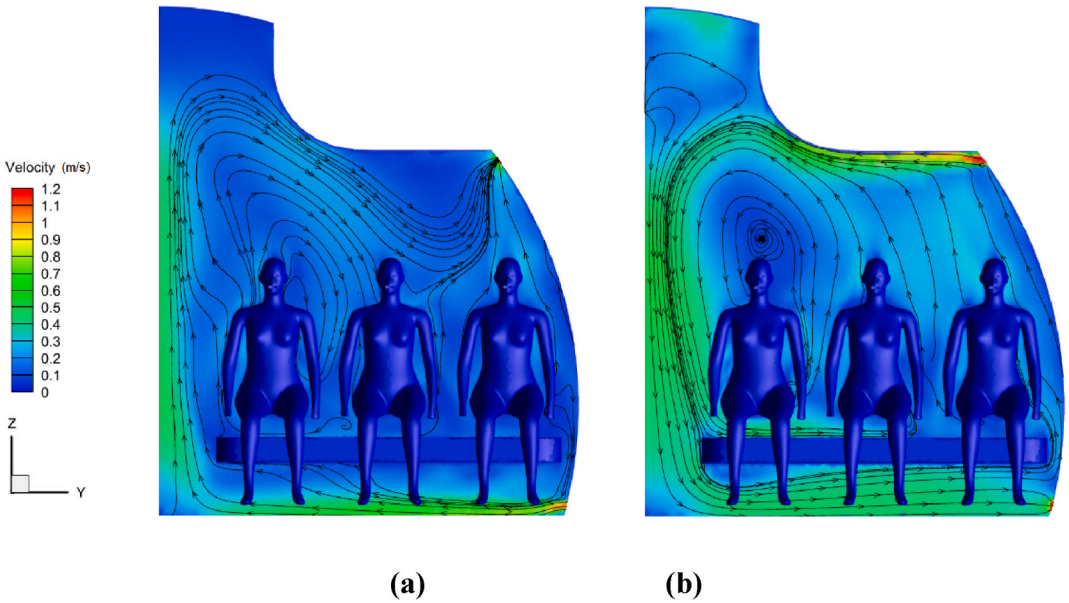

Fig. 6. Contours of the air flow velocity field. (a)DV system, (b) MV system.

experiment results are based on similar cabin structures. The differences in calculation results were found to be mainly due to the difference in symmetry condition and details of the geometric model.

The direction of the flow field in the mixing ventilation (MV) system (Fig. 6 (b)) appears opposite in situation to the DV system. It was also found that in the DV system, there is a larger flow rate near the floor, while in the MV system, the larger flow rate appears under the baggage compartment (Fig. 8 (a)&(b)). The flow field on the left side of the passenger in the C2 position (Fig. 1) moves downwards, flowing out of the cabin space from the bottom of the seat. In Fig. 8 (c), two points, L4 and L5, directly in front of the passenger in position 2B were monitored in the ventilation system's steady state. L4 was 120 mm away from the center of the passenger's mouth in position 2B (Fig. 1), and L5 was 360 mm away from the same passenger's mouth.

3.2. The dispersion of suspending droplets in the displacement ventilation system and the mixing ventilation system

Comparing the results shown in Fig. 9, the transient dispersion of different sized droplets in the environment was found to show significant differences; The way droplets spread determines the safe distance between the infected passengers and the uninfected passengers. There are many factors that affected the droplets' distance of travel, such as the heat plume of human body, and ambient wind, but the biggest influencing factor in the early stage was the air flow generated by cough.

After examining the dispersion of various droplets diameter droplets in the cabin (Fig. 9 (a) & (b)), large droplets of initial diameter 100 μm almost completely escaped from exhaust or trapped on the wall in the DV system. But large droplets under the MV system were partially settled and re-blown to the upper cabin by updrafts, which increased the probability of droplet dispersion of large diameter droplets.

The droplets of initial diameter 10 μm spread more uniformly in the flow field, which also made this (medium) size of droplet the most powerful carrier of the COVID-19 virus. It can also be seen from Fig. 9 (c) and (d) that the DV system had more suspended droplets than the MV system in the passenger's inhalation area.

As shown in Fig. 9 (e) and (f), droplets of initial diameter 1 μm were found to spread slower after outflow, and under the DV system, these smaller droplets tended to accumulate on the cabin window, affecting the respiratory safety of passengers on the inner seats. Under the MV system, the smaller diameter droplet migrates toward the upper space of the cabin.

3.3. Comparison of the fate of droplets in different ventilation systems

To compare the number of suspended droplets under the two ventilation systems, the number of droplets of each diameter was normalized relative to the initial number. In order to measure the statistical results of the fate of droplet pollutants of various diameters in different cabin ventilation systems, we calculated the droplet propagation in the cabin according to the initial diameter distribution of a fixed number of particles. Limited by compute resources, the simulation time was limited to 400s for all cases in Fig. 10. In the DV system, the largest droplet with an initial diameter of 100 μm completely settled or escaped within 8s, and the medium droplet with an initial diameter of 5 μm basically settled or escaped within 110s, while 3.52% of the small droplets with initial diameter of 1 μm remained in the air at 400s. In the MV system, 1% of the large droplets with an initial diameter of 100 μm remained in the air after 30s, and all droplets with a medium initial diameter escaped or settled within 140s. However, 24.26% of all droplets with an initial diameter of 1 μm still remained suspended in the air at 400s.

The fraction of droplets remaining suspended for each initial diameter of droplets was recorded, and Fig. 10 compares the number of suspended droplets in the air of the two ventilation systems. It was found that the DV system is generally better than the MV system over the equal durations in escaping or settling droplets. The escape or sedimentation behavior of different initial diameter droplets meant obvious advantages in the DV system.

Comparing the fate of droplets in the two ventilation systems in Fig. 11, it was found that the number of suspended droplets on the

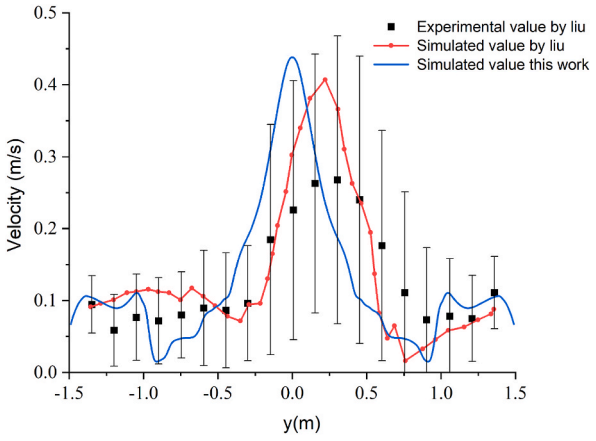

Fig. 7. Velocity comparison of 1.2 m height in the DV system flow field.

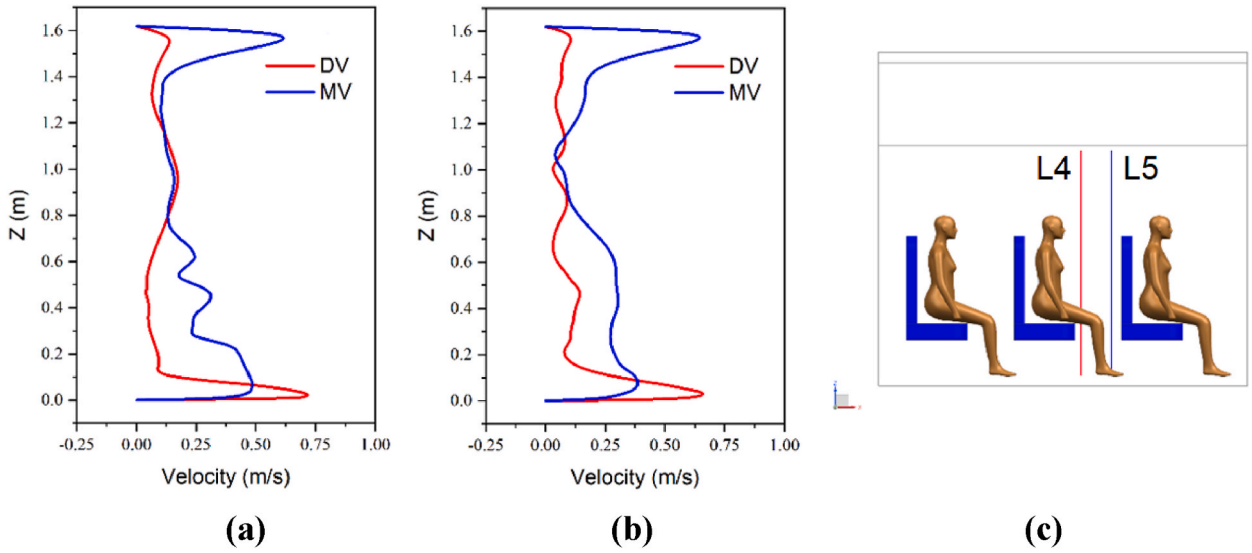

Fig. 8. Velocity monitoring at L4 and L5 in the flow field. (b) L4, (b) L5, (c) Diagrammatize.

DV system was lower than the initial release quantity, and the DV system is more conducive to the trap or escape of droplets in the aircraft cabin. This is also consistent with previous studies. The droplets suspended in the DV system was 11.07% less than those in the MV system at 10s from the start of droplet release. In addition, the number of droplets that escaped through the exhausts in the DV system was 13.15% more in the DV system than in the MV system at 400s. The statistical results only include the droplets of monodisperse distribution.

3.4. Infection probability in different ventilation systems

The statistical results of infection probability of DV system and MV system at different positions are shown in Fig. 12. The infection probability of passengers in DV system is higher than that in MV system in some positions, and the infection probability in window position 1A, 2A and 3A is higher than that in MV system. However, the risk at position 1C, 2C, 3C near the channel was significantly higher in the MV system than in the DV system. This result is due to the flow field inside the ventilation system; The DV system concentrates the droplets on the side near the window easier than the MV system.

For rear passengers, the DV system is superior to the MV system only in the aisle. In general, DV system can remove pollutants better than MV system. From the perspective of the risk of contamination in the passenger inhalable area, DV system is not superior to MV system locally. The statistical results only include the droplets of monodisperse distribution.

3.5. Influence of inlet velocity on infection probability in DV system

By changing the inlet velocity of DV system, the influence of the air mass flow rate of ventilation system on the infection risk of passengers was studied. Fig. 13 shows the comparison of infection risk of passengers in DV system when the inlet velocity is 0, 0.5, 1 and 1.5 m/s respectively.

Fig. 13(a) shows the maximum risk at 1 m/s as the DV system inlet velocity increases. For passengers near aisle 1C, the minimum value was 1 m/s, and the infection probability increased by 22.21% when the wind velocity continued to increase to 1.5 m/s. As can be seen from Fig. 13(b), the infection probability of passengers does not decrease with the increase of wind velocity. After the increase from 1 m/s to 1.5 m/s, the infection risk of passengers on both sides of the infected person has different changes. The infection probability of passengers decreases by 9.14% at 2A, while it increases by 11.44% at 2C. This could be attributed to the complex geometry of the cabin, resulting in changes in the direction of air flow. In Fig. 13(c), the infection rate remained high even for rear passengers without ventilation system. The infection risk of infected passengers in the rear row decreased with the increase of wind velocity, and the increase of wind velocity in the ventilation system reduced the possibility of droplet pollution spreading to the rear row.

Compared with the condition without ventilation system, increasing the air flow rate of DV system effectively reduces the probability of infection of passengers, especially in the rear seat. The high inlet velocity is conducive to the overall reduction of suspended droplets in the air. However, the intensification of air flow rate in the cabin increases the proportion of droplets in the passenger inhalation area in some positions, due to the complex flow field structure, and different turbulence intensity. The statistical results only include the droplets of monodisperse distribution.

By changing the inlet air velocity of the DV system, the effect of the ventilation system inlet velocity on the discharge of droplet pollutants was studied. The statistical results covered droplets of all diameter sizes. The fate of droplets at different inlet velocities are

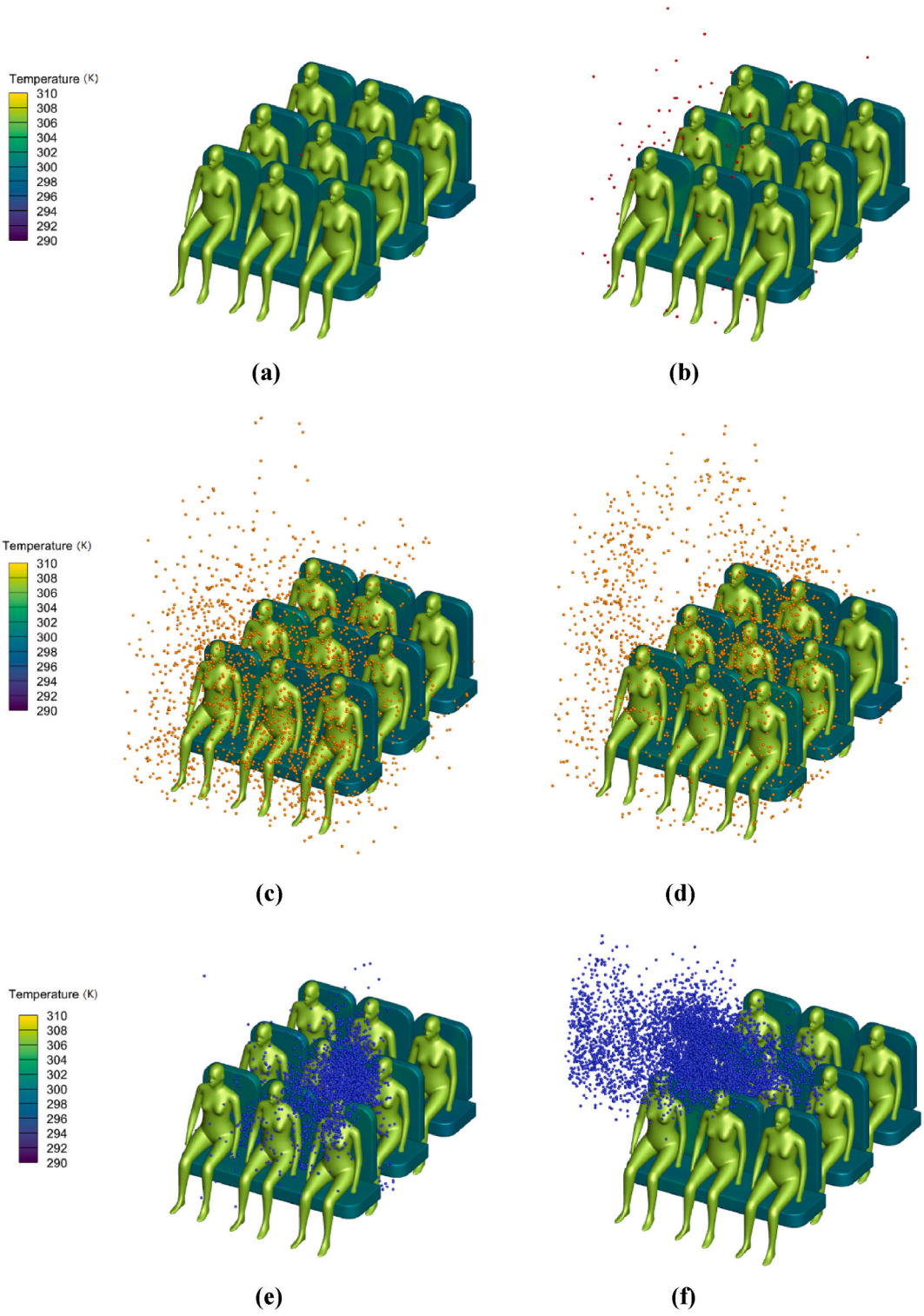

Fig. 9. Snapshot of droplets with different diameter at t = 24s. (a)Initial diameter of 100 μm in DV system, (b) Initial diameter of 100 μm in MV system, (c)Initial diameter of 10 μm in DV system, (d) Initial diameter of 10 μm in MV system, (e)Initial diameter of 1 μm in DV system, (f) Initial diameter of 1 μm in MV system.

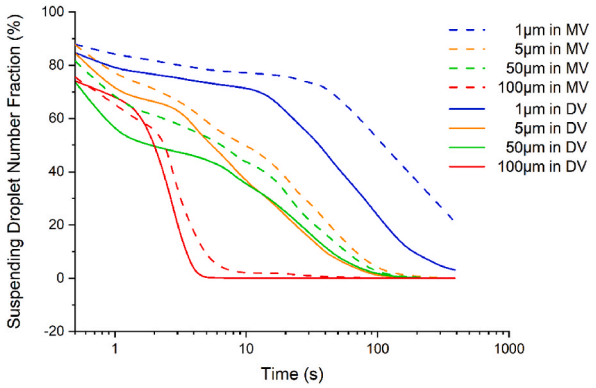

Fig. 10. Number fraction of suspending droplet with different initial diameters.

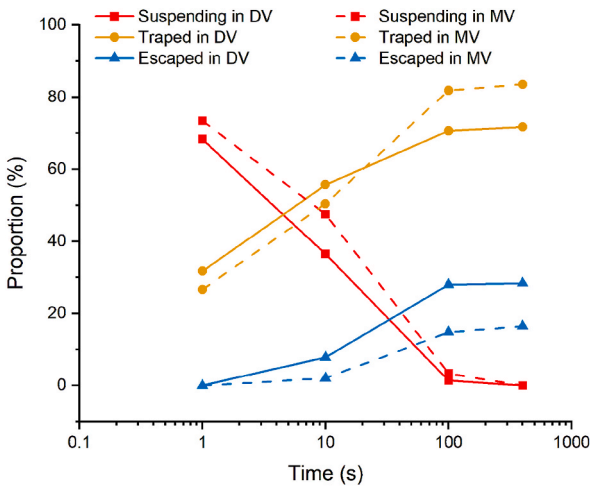

Fig. 11. The fate of droplets in different ventilation systems.

compared in Fig. 14. The number of suspended droplets was greatest, when ventilation is not used. At 400s, the number of droplets escaped from the outlet was largest with an inlet velocity of 1 m/s. It was also found that the proportion of droplets suspended in the air was the lowest at the same time point when the inlet velocity was 1.5 m/s. This might be due to the increased rate of gas displacement in the aircraft cabin. The statistical results only include the droplets of monodisperse distribution.

4. Conclusions

In this study, two aircraft cabin ventilation systems were analyzed from the perspective of dynamic droplet dispersion. When compared with previous studies of cough droplets in an enclosed space, it was found that the dispersion results of droplets in different ventilation environments have a huge difference. This was mainly determined by the ventilation system and complex geometric space composed of the cabin and passengers. The simplified polydisperse droplets were tracked and the results also showed that their dispersion results were significantly different from those in a poorly ventilated environment.

Our research presents some unique points, arguing that in a crowded cabin environment, the use of ventilation systems locally increases the infection probability. After exploring the displacement ventilation system's inlet velocity, it was learned that higher inlet velocity can be used to improve the efficiency of a displacement ventilation (DV) system in reducing suspended droplets, which is consistent with literature records. In addition, the droplets suspended in the DV system were 11.07% lower than those in a mixing ventilation (MV) system at 10s from the start of the droplet releasing. The number of droplets escaped through the exhausts in the DV system was also 13.05% more than in the MV system at 400s.

By using the CFPD method to visualize the trajectory and fate of virus-laden droplets under ventilation environmental conditions and to simulate the condensation/evaporation effect between environmental water vapor and droplets, we made some novel findings: (1) Large droplets that settle rapidly in a windless environment may be re-lifted by the ambient wind in an MV system and eventually taken to the occupant's inhalation area. (2) DV systems work better than MV systems in reducing suspended droplets, but the probability of infection of local passengers by the window positions in a DV system is greater than in MV systems. (3) Increasing the wind

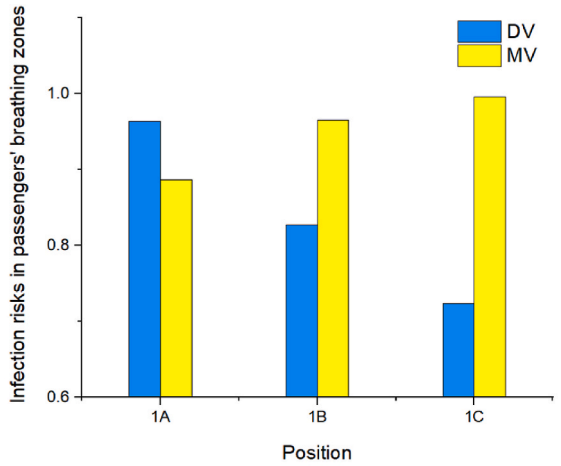

(a)

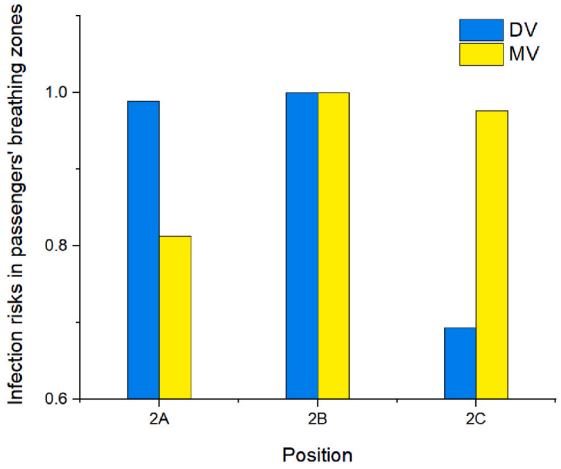

(b)

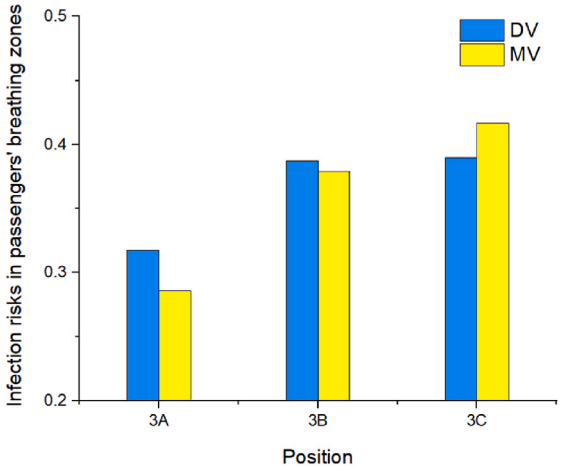

(c)

Fig. 12. Risk probability of infection of passengers at each location under two ventilation systems. (a)Row1, (b) Row2, (c) Row3.

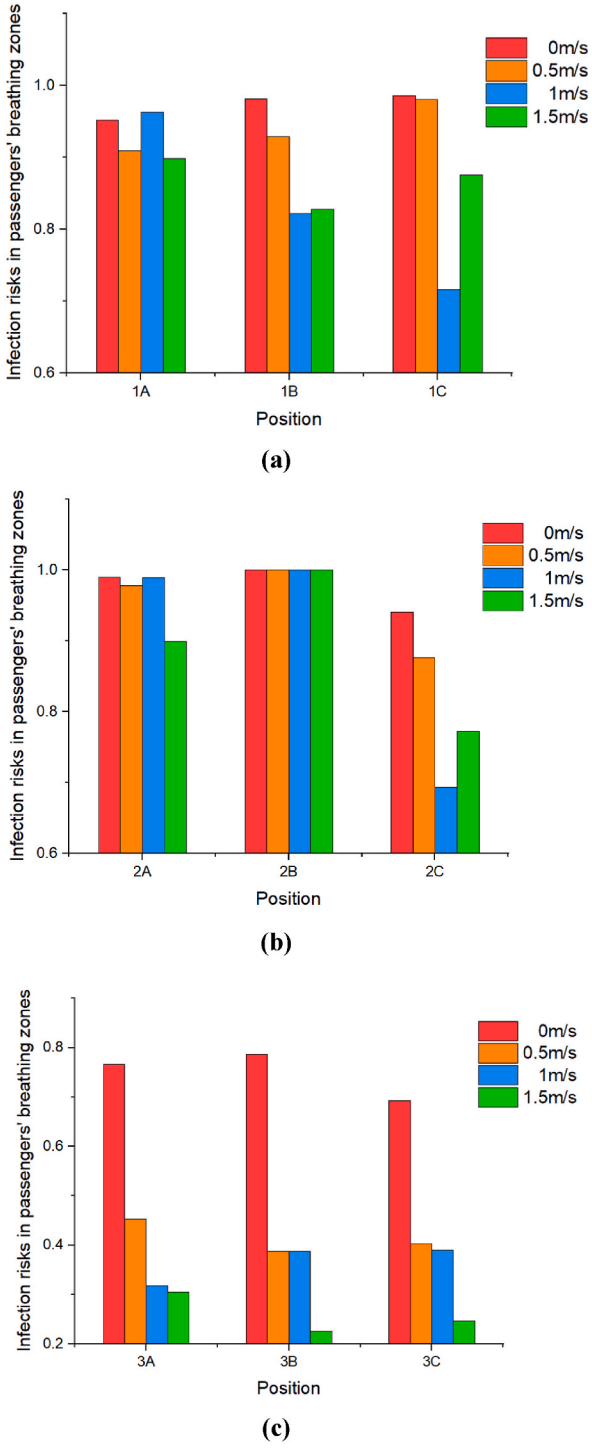

Fig. 13. Risk probability of passenger infection at different flow velocities. (a) Row1, (b) Row2, (c) Row3.

velocity of a DV system can accelerate the reduction of the number of suspended droplets in the air, but it will also increase the degree of droplets diffusion and increase the probability of infection at some locations.

In future studies, experimental studies on sneeze shields/guards will be conducted to further investigate their effects on cabin airflow, especially in relation to passenger comfort and noise generation. The effect of evaporation of the deposited droplets on virus transmission will also be further investigated experimentally.

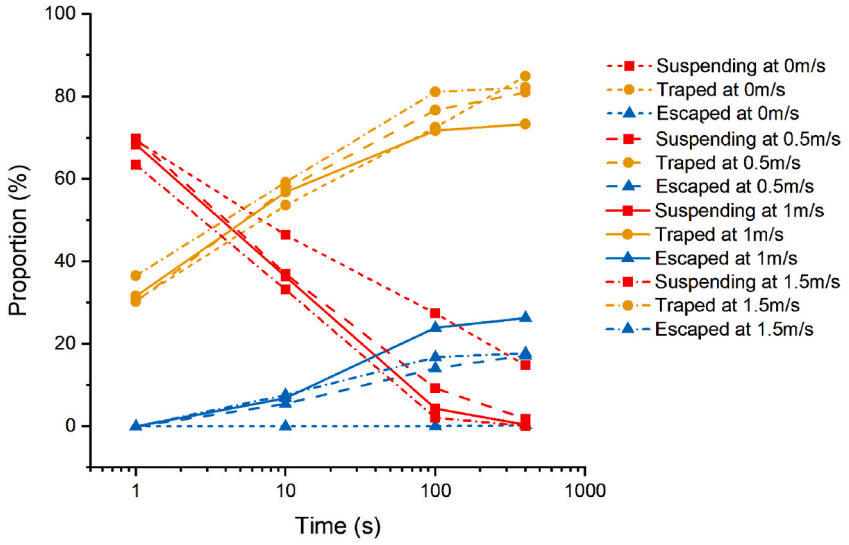

Fig. 14. The fate of droplets at different inlet velocities.

Author contribution statement

Zhuxun Liu: Performed the experiments; Analyzed and interpreted the data; Wrote the paper.
Jingyi Wu: Conceived and designed the experiments; Analyzed and interpreted the data.
Guang Yang: Conceived and designed the experiments.
Xintai Zhang: Performed the experiments, Contributed reagents, materials, analysis tools or data.
Zheng Dai: Contributed reagents, materials, analysis tools or data.

Funding statement

This research did not receive any specific grant from funding agencies in the public, commercial, or not-for-profit sectors.

Data availability statement

Data will be made available on request.

Declaration of interest's statement

The authors declare no conflict of interest.

References

[1] L. Moravian, Droplet fate in indoor environments, or can we prevent the spread of infection? J. Indoor Air 16 (5) (2006) 335–347.
[2] A. Pavli, P. Smeti, S. Hadjianastasiou, K. Theodoridou, A. Spilioti, K. Papadima, A. Andreopoulou, K. Gkolfinopoulou, S. Sapounas, N. Spanakis, A. Tsakris, H. C. Maltezou, In-flight transmission of COVID-19 on flights to Greece: an epidemiological analysis, J. Travel Med. Inf. Disp. 38 (2020), 101882.
[3] P. Christidis, A. Christodoulou, The predictive capacity of air travel patterns during the global spread of the COVID-19 pandemic: risk, uncertainty and randomness, J. Int. J. Environ. Res. Publ. Health 17 (10) (2020) 3356.
[4] L. Schibuola, C. Tambani, High energy efficiency ventilation to limit COVID-19 contagion in school environments, J. Energy Build 240 (2021). Article 110882.
[5] P.S. Desai, N. Sawant, A. Keene, On COVID-19-safety ranking of seats in intercontinental commercial aircrafts: a preliminary multiphysics computational perspective, medRxiv 14 (6) (2020) 1585–1596.
[6] D. Bhatia, A. De Santis, A preliminary numerical investigation of airborne droplet dispersion in aircraft cabins, J. Open J. Fluid Dynam. 10 (3) (2020) 198–207.
[7] C.Y.H. Chao, M.P. Wan, L. Morawska, G.R. Johnson, Z.D. Ristovski, M. Hargreaves, K. Mengersen, S. Corbett, Y. Li, X. Xie, D. Katoshevski, Characterization of expiration air jets and droplet size dispersions immediately at the mouth opening, J. Aerosol Sci. 40 (2009) 122–133.
[8] John Redrow, Shaolin Mao, Ismail Celik, J. Alejandro Posada, Zhi-gang Feng, Modeling the evaporation and dispersion of airborne sputum droplets expelled from a human cough, J. Build. Environ. 46 (Issue 10) (2011) 2042–2051. ISSN 0360-1323.
[9] F. Schaffer, M. Soergel, D. Straube, Survival of airborne influenza virus: effects of propagating host, relative humidity, and composition of spray fluids, J. Arc. Virol. 51 (1976) 263–273.
[10] Christian Lieber, Stefanos Melekidis, Rainer Koch, Hans-Jörg Bauer, Insights into the evaporation characteristics of saliva droplets and aerosols: levitation experiments and numerical modeling, J. Aer. Sci. 154 (2021), 105760. ISSN 0021-8502.
[11] Gang Zeng, Lin Chen, Haizhuan Yuan, Ayumi Yamamoto, Shigenao Maruyama, Evaporation flow characteristics of airborne sputum droplets with solid fraction: effects of humidity field evolutions, J. Phy. Fluids 33 (2021), 123308, https://doi.org/10.1063/5.0076572.
[12] Yi Y. Zuo, et al., William E. Uspal, and tao wei airborne transmission of COVID-19: aerosol dispersion, lung deposition, and virus-receptor interactions, J. ACS Nano 14 (12) (2020) 16502–16524, 2020.

[13] Li Yan, Y. Yan, X. Li, J. Tu Thermal effect of human body on cough droplets evaporation and dispersion in an enclosed space, Tu, 2019, J. Build. Environ. 148 (2019) 96–106, https://doi.org/10.1016/j.buildenv.2018.10.039.
[14] K. Inthavong, Q.J. Ge, X.D. Li, J.Y. Tu, Detailed predictions of particle aspiration affected by respiratory inhalation and airflow, J. Atmos. Environ. 62 (2012) 107–117.
[15] T.P. Weber, N. I, Stilianakis Inactivation of influenza A viruses in the environment and modes of transmission: a critical review, J. Infect. 57 (2008) 361–373.
[16] J. Gralton, E. Tovey, M.L. McLaws, W.D. Rawlinson, The role of particle size in aerosolised pathogen transmission: a review, J. Infect. 62 (2011) 1–13.
[17] D. Silcott, S. Kinahan, J. Santarpia, B. Silcott, R. Silcott, P. Silcott, B. Silcott, S. Distelhorst, V. Herrera, D. Rivera, K. Crown, G. Lucero, W. Bryden, M. McLoughlin, M. Cetta, R. Accardi, TRANSCOM/AMC Commercial Aircraft Cabin Aerosol Dispersion Tests, 2020.
[18] I. Baumann, M. Trimmel, Dispersion of subjective assessments in a controlled aircraft environment, J. Aero. Sci. Technol. 25 (1) (2013) 93–101.
[19] A. Mangili, M.A. Gendreau, Transmission of infectious disease during commercial air travel, J. Lancet 365 (9463) (2005) 989–996.
[20] Y. Zhang, J. Liu, J. Pei, J. Li, C. Wang, Performance evaluation of different ventilation systems in an aircraft cabin mockup, J. Aero. Technol. 70 (2017) 359–366.
[21] R. You, Chao-Hsin Lin, D. Wei, Q. Chen, Evaluating the commercial airliner cabin environment with different ventilation systems, J. Indoor Air 29 (2019) 840–853.
[22] Chanfiou Ahmed Mboreha, Xavier Tytelman, Nwaokocha Collins, Abayomi Layeni, Ruth C. Okeze, Abdalah Shaibu Amiri Numerical simulations of the flow fields and temperature dispersion in a section of a Boeing 767–300 aircraft cabin, Mater. J. Today: Proceedings 47 (2021) 4098–4106. Part 13.
[23] Qing Cao, Ming xin Liu, Xing yang Li, Chao-Hsin Lin, Daniel Wei, Sheng cheng Ji, Teng fei (Team) Zhang, Qing yan Chen Influencing factors in the simulation of airflow and droplets transportation in aircraft cabins by CFD, Part B, J. Build. Environ. 207 (2022), 108413. ISSN 0360-1323.
[24] J. Maier, C. Marggraf-Micheel, F. Zinn, T. Dehne, J. Bosbach Ceiling-based cabin displacement ventilation in an aircraft passenger cabin: analysis of thermal comfort, [J. Build. Environ. 146 (2018) 29–36.
[25] Z. Zhang, X. Chen, S. Mazumdar, T. Zhang, Q. Chen, Experimental and numerical investigation of airflow and contaminant transport in an airliner cabin mockup, J. Build. Environ. 44 (1) (2009) 85–94.
[26] W. Yan, Y. Zhang, Y. Sun, D. Li, Experimental and CFD study of unsteady airborne pollutant transport within an aircraft cabin mock-up, J. Build. Environ. 44 (1) (2009) 34–43.
[27] J.K. Gupta, C.H. Lin, Q. Chen, Transport Of Expiratory Droplets In An Aircraft Cabin Indoor Air, 2011, pp. 3–11, 21 (1).
[28] J.K. Gupta, C.H. Lin, Q. Chen, Risk Assessment Of Airborne Infectious Diseases In Aircraft Cabins Indoor Air, 2012, pp. 388–395, 22 (5).
[29] Y. Yan, X. Li, Y. Shang, J. Tu, Evaluation of airborne disease infection risks in an airliner cabin using the Lagrangian-based Wells-Riley approach, J. Build. Environ. 121 (2017) 79–92.
[30] C.A. Mboreha, S. Jianhong, W. Yan, S. Zhi, Z. Yantai, Investigation of thermal comfort on innovative personalized ventilation systems for aircraft cabins: a numerical study with computational fluid dynamics, Therm. Sci. Eng. Prog. 26 (December 2021) (2021), 101081.
[31] H. Ahn, D. Rim, L.J. Lo, Ventilation and energy performance of partitioned indoor spaces under mixing and displacement ventilation, Build. Simul. 11 (2018) 561–574.
[32] X. Shan, J. Zhou, V.W.C. Chang, E.H. Yang, Comparing mixing and displacement ventilation in tutorial rooms: studentsthermal comfort, sick building syndromes, and short-term performance Build, Environ. Times 102 (2) (2016) 128–137.
[33] X. Li, T.T. Zhang, M. Fan, M. Liu, D. Chang, Z.D. Wei, C.H. Lin, S. Ji, J. Liu, S. Shen, Z. Long, Experimental evaluation of particle exposure at different seats in a single-aisle aircraft cabin Build, Environ. Times 202 (2021). Article 108049.
[34] Xiangdong Li, Yihuan Yan, Jiyuan Tu, The simplification of computer simulated persons (CSPs) in CFD models of occupied indoor spaces, J. Build. Environ. 93 (2015) 155–164. Part 2.
[35] J. Zhao, Y. Feng, M. Bezerra, J. Wang, T. Sperr umerical simulation of welding fume lung dosimetry, J. Aerosol Sci. 135 (2019) 113–119, https://doi.org/10.1016/j.jaerosci.2019.05.006.
[36] Feng Yu, Thierry Marchal, Ted Sperry, Hang Yi, Influence of wind and relative humidity on the social distancing effectiveness to prevent COVID-19 airborne transmission: a numerical study, J. Journal of Aerosol Science 147 (2020), 105585, 0021-8502.
[37] Y. Feng, C. Kleinstreuer, N. Castro, A. Rostami, Computational transport, phase change and deposition analysis of inhaled multicomponent droplet–vapor mixtures in an idealized human upper lung model, J. Aerosol Sci. 96 (2016) 96–123.
[38] A. Banko, F. Coletti, D. Schiavazzi, C. Elkins, J. Eaton, Three-Dimensional Inspiratory Flow In The Upper And Central Human Airways Experiments In Fluids, 2015, p. 117, 56 (6).
[39] J. Li, X. Cao, J. Liu, C. Wang, Y. Zhang, Global airflow field distribution in a cabin mock-up measured via large-scale 2D-PIV, J. Build. Environ. 93 (2015) 234–244.
[40] ASHREA Air Quality within Commercial Aircraft, ANSI/ASHREA Standard 161–2007 American Society of Heating, Refrigerating and Air Conditioning Engineers, Inc., Atlanta, 2007.
[41] W. Cui, Q. Ouyang, Y. Zhu, Field study of thermal environment spatial distribution and passenger local thermal comfort in aircraft cabin Build, Environ. Times 80 (2014) 213–220.
[42] J. Wei, Y. Li, Enhanced spread of expiratory droplets by turbulence in a cough jet, J. Build. Environ. 93 (2015) 86–96.
[43] X. Li, Y. Shang, Y. Yan, L. Yang, J. Tu, Modelling of evaporation of cough droplets in inhomogeneous humidity fields using the multi-component Eulerian-Lagrangian approach, J. Build. Environ. 128 (2018) 68–76.
[44] D. Licina, A. Melikov, C. Sekhar, K.W. Tham, Human convective boundary layer and its interaction with room ventilation flow, J. Indoor Air 25 (1) (2015) 21–35.
[45] A. Haghnegahdar, J. Zhao, Y. Feng Lung aerosol dynamics of airborne influenza A virus-laden droplets and the resultant immune system responses: an in silico study, J. Journal of Aerosol Science 134 (2019) 34–55, https://doi.org/10.1016/j.jaerosci.2019.04.009.
[46] N. Sen, Transmission and evaporation of cough droplets in an elevator: numerical simulations of some possible scenarios, [J. Phys. Fluids 33 (3) (2021), 033311.
[47] Amit Agrawala and Rajneesh Bhardwaja Probability of COVID-19 infection by cough of a normal person and a super-spreader featured, J. Physics of Fluids 33 (2021), 031704.
[48] E.C. Riley, G. Murphy, R.L. Riley, Airborne spread of measles in a suburban elementary school, Am. J. Epidemiol. 107 (1978) 421–432.
[49] H. Qian, Y. Li, P.V. Nielsen, X. Huang, Spatial distribution of infection risk of SARS transmission in a hospital ward, Build. Environ. 44 (8) (2009) 1651–1658.
[50] R. You, C.H. Lin, D. Wei, Q. Chen, Evaluating the commercial airliner cabin environment with different air distribution systems, Indoor Air 29 (5) (2019) 840–853.
[51] Mingxin Liu, Junjie Liu, Qing Cao, Xingyang Li, Sumei Liu, Shengcheng Ji, Chao-Hsin Lin, Daniel Wei, Xiong Shen, Zhengwei Long, Qingyan Chen, Evaluation of different ventilation systems in a commercial airliner cabin in terms of comfort and COVID-19 infection risk, J. Build. Environ. 208 (2022), 108590, 0360-1323.
[52] K. Talaat, M. Abuhegazy, O.A. Mahfoze, O. Anderoglu, S.V. Poroseva, Simulation of aerosol transmission on a Boeing 737 airplane with intervention measures for COVID-19 mitigation, Phys. Fluids 33 (2021), 033312.
[53] P. Zítek, T. Vyhlídal, G. Simeunović, et al., Novel personalized and humidified air supply for airliner passengers, J. Build. Environ. 45 (11) (2010) 2345–2353.
[54] W. Liu, J. Wen, C.H. Lin, et al., Evaluation of various categories of turbulence models for predicting air distribution in an airliner cabin, J. Build. Environ. 65 (2013) 118–131.